High-resolution angle-resolved photoemission investigation of the electronic structure of Cr-intercalated 1*T*-$TiTe_2$

T. V. Kuznetsova, A. N. Titov,* Yu. M. Yarmoshenko, E. Z. Kurmaev, and A. V. Postnikov†
Institute of Metal Physics, RAS Ural Division, 620219 Yekaterinburg GSP-170, Russia

V. G. Pleschev
Ural State University, 620083 Yekaterinburg, Russia

B. Eltner, G. Nicolay, D. Ehm, S. Schmidt, F. Reinert,‡ and S. Hüfner
Universität des Saarlandes, Fachrichtung Experimentalphysik, D-66041 Saarbrücken, Germany
(Received 1 March 2005; published 4 August 2005)

We report the results of the study by angle-resolved photoelectron spectroscopy of intercalated compound $Cr_{1/3}TiTe_2$. In the range of binding energies up to 6 eV we obtained band mapping along Γ-M, Γ-M', and M-K directions of the Brillouin zone. It was established that electronic structure of $TiTe_2$ changes substantially under the inclusion of Cr. An additional, essentially dispersionless band appears at ~1 eV below the Fermi level. Band structure calculations allow one to interpret this band as being due to the Cr3*d*-Ti3*d* mixed states. An almost dispersionless character of this band allows one to presume a polaronlike nature of Cr-Ti mixed states.

DOI: 10.1103/PhysRevB.72.085418 PACS number(s): 79.60.−i, 71.20.−b, 71.55.−i, 87.64.Lg

I. INTRODUCTION

Intercalation compounds based on titanium dichalcogenides with a generic formula M_xTiX_2 (M, intercalating 3*d* element, Cr to Ni; X, S, Se or Te) are layered materials, in which M atoms occupy (either randomly or in an ordered way) empty spaces between repeated layers of a host dichalcogenide. These materials resemble (in what regards anisotropy of elastic, magnetic and transport properties) artificial multilayer systems, in which thin layers of magnetic metal are separated by nonmagnetic blocks.

The magnetic moment of an "impurity" M is determined by its valence state and hence by the chemical bonding between the intercalating element and the host lattice. Such bonding is well studied for intercalate compounds with alkali metals, where the host lattice acquires extra electron density and fixes the ionized guest species electrostatically. In the case of inserted 3*d* elements this simple picture does not work, as magnetic moments of impurity atoms deviate considerably from free-ion values. Moreover the interlayer distances do not increase on doping, as in the case of alkali metals, but on the contrary get smaller. As was shown in Ref. 1, the compression of interlayer distances on 3*d* intercalation of $TiSe_2$ correlates with the ionization potential of the inserted ion. One could describe this relation quantitatively, assuming the formation of a narrow band (of localized impurity states) just below the Fermi energy. Indeed, angle-resolved photoelectron spectroscopy (ARPES) indicated the formation of such bands for some TiS_2-based intercalate compounds,[2,3] notably in those cases when the intercalation resulted in the decrease of interplanar distances.[4] Such bands are situated 0.5 to 1 eV below the Fermi level and exhibit no dispersion, thus indicating a considerable localization of corresponding states. However the mechanism of so strong localization of the states with the energies so close to the Fermi level remained obscure.

Another group of materials where one observed similar dispersionless bands close to the Fermi level are cuprate high-temperature superconductors.[5] In Ref. 6 the presence of such bands was explained by the formation of polarons in the Cu-O planes. It seems plausible for the same mechanism to play a role in intercalated compounds. Polarons may appear as a result of a local distortion in the vicinity of an impurity atom, as an electron gets captured by the hybridized (Ti3*d*,*M*3*d*) band. In fact, phase diagrams of M_xTiX_2 (M=Ag,Fe,Co,Cr; X=Se,Te) were satisfactorily explained under assumption of a polaronic nature of the hybride states.[7] A signature of this mechanism is that the localization would grow with the lattice polarizability. Among chalcogenides, the polarizability is the largest in tellurides. We are not aware of previous ARPES studies of 3*d*-intercalated $TiTe_2$. In the present contribution we report the experimental spectra and the discussion for one such (ordered) compound, $Cr_{1/3}TiTe_2$.

II. EXPERIMENTAL DETAILS

Polycrystalline samples Cr_xTiTe_2 were obtained by a standard procedure of ampoule synthesis from constituent elements. In order to prevent the effect of chromium ordering on the electronic structure, the samples were quenched from temperatures above 850 °C. The synthesis and characterization of samples are discussed in details in Ref. 8. The applied heat treatment allowed to prevent the ordering of intercalant in all samples with the exception of $Cr_{1/2}TiTe_2$ where a superstructure $a_0 \times a_0\sqrt{3} \times 2c_0$ has been observed, that corresponds to the lowering of the space group symmetry from $P\bar{3}m1$ to $I2/m$. The corresponding hexagonal unit cell and the Brillouin zone (BZ) of $TiTe_2$ are depicted in Fig. 1. The parameters a_0, c_0 of hexagonal Cr_xTiTe_2 lattice in their dependence on the Cr composition, as determined from x-ray

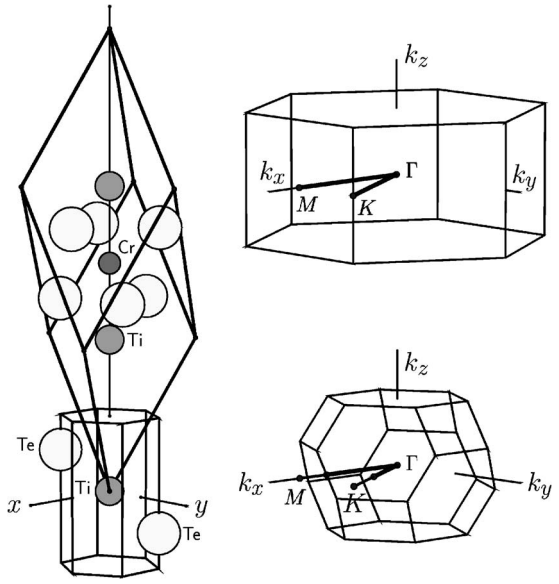

FIG. 1. Left-hand panel, hexagonal Wigner-Seitz cell of $TiTe_2$ and rhombohedral primitive cell of ordered $CrTi_3Te_6$. Right-hand panel, Brillouin zone of $TiTe_2$ (top) and $CrTi_3Te_6$ (bottom). *M* and *K* special points are shown in both cases in the hexagonal setting. The part of *M*-Γ-*K* path within the Brillouin zone of the rhombohedral supercell is shown by a thicker line.

powder diffraction analysis using the DRON-4-13 diffractometer (Co K_α radiation, planar graphite monochromator), are shown in Fig. 2. An increase of the chromium content up to $Cr_{1/2}TiTe_2$ is accompanied by a smooth change of lattice parameters, that, along with the absence of other phases, witnesses a good chromium solubility at least up to $x=0.33$.

The samples for spectroscopic investigations were grown as monocrystalline by a gas-transport reaction using I_2 as a carrier. For the details of the synthesis procedure see Ref. 8. The chromium content in the monocrystals thus grown has been determined from the concentration dependence of lattice parameters, calibrated earlier for polycrystalline samples. Independently, chemical composition of monocrystals has been tested with an x-ray microanalyzer JEOL-733. Both methods confirmed the identical composition of all obtained monocrystals, $Cr_{1/3}TiTe_2$.

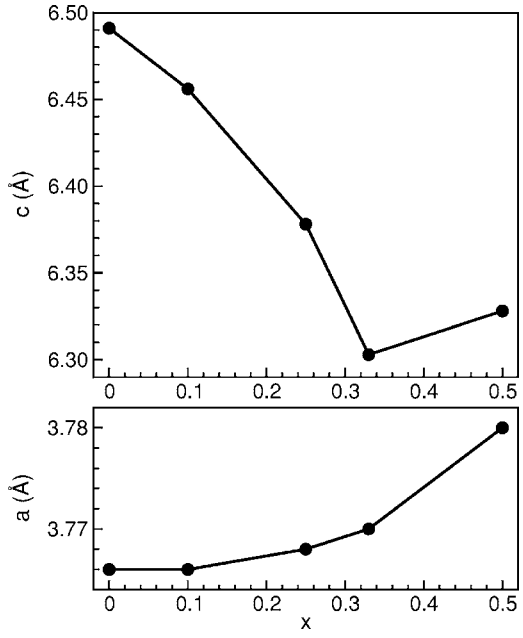

FIG. 2. Lattice constants of $TiTe_2$ as function of composition of inserted Cr, obtained from x-ray diffraction for powder samples.

High-resolution angle-resolved photoelectron spectroscopy experiments have been performed with a SCIENTA SES 200 spectrometer using monochromatized GAMMA-DATA VUV-lamp with $h\nu=21.23$ eV (He I). The base pressure in the analyzer chamber was 3×10^{-11} mbar. The energy resolution of the analyzer system $\delta E=5$ meV was estimated by measuring the Fermi edge of a cooled silver sample; the angle resolution was better than 0.5° ($\delta k_\parallel < 0.03$ Å^{-1}) in the dispersive direction. The sample temperature was maintained below 10 K. The samples were cleaved in ultrahigh vacuum of the analyzer chamber. Single-crystal samples were oriented using x-ray Laue diffraction prior to being inserted into the chamber. The electron density analyzer was mounted statically while the sample holder rotated to scan the emission directions relative to the crystal axis. The cleanness of the sample surface was controlled by measuring the oxygen 1*s* x-ray photoelectron spectra before and after the ARUPS measurements. A more detailed description of experimental conditions can be found in Ref. 9.

III. BAND STRUCTURE CALCULATIONS

The electronic structure of pure and doped 1*T*-$TiTe_2$ has been simulated in a supercell calculation with the use of the density functional theory (DFT). Specifically, we applied the full-potential augmented plane wave method as implemented in the WIEN2K package.[10] The calculation treated exchange correlation in the generalized gradient approximation after Perdew-Burke-Ernzerhof.[11] Our primary aim was to establish a relation between band dispersions as found in the calculation, on the one hand, and probed by the spectroscopic experiment, on the other hand. The intercalated system $Cr_{1/3}TiTe_2$ was represented in our calculation by an ordered rhombohedral supercell $Cr(TiTe_2)_3$ (Fig. 1), similar to that used by Matsushita *et al.*,[3] and in our earlier work.[8,12] The experimental band structure, both with and without Cr doping, is only accessible in the setting corresponding to the hexagonal $TiTe_2$ crystal. For better understanding of calculated band structures related to the BZ of $TiTe_2$ we considered, along with the standard hexagonal unit cell, a rhombohedrically tripled cell also without the intercalating chromium. The relation between BZs of pristine $TiTe_2$ and rhombohedral $Cr_{1/3}TiTe_2$ is shown in Fig. 1, where we emphasize the directions in the *k* space along which the measured and calculated band structures become available. Other (different) illustrations of the BZ folding for a case isostructural to ours, TiS_2 vs $M_{1/3}TiS_2$, can be found in Fig. 1 of Ref. 13 and Fig. 2 of Ref. 3.

The following experimentally measured lattice vectors and internal parameters were used: $a=3.777$ Å, $c=6.498$ Å, $z=0.2628$ for pure $TiTe_2$ and $a=3.8627$ Å, $c=6.3461$ Å, z

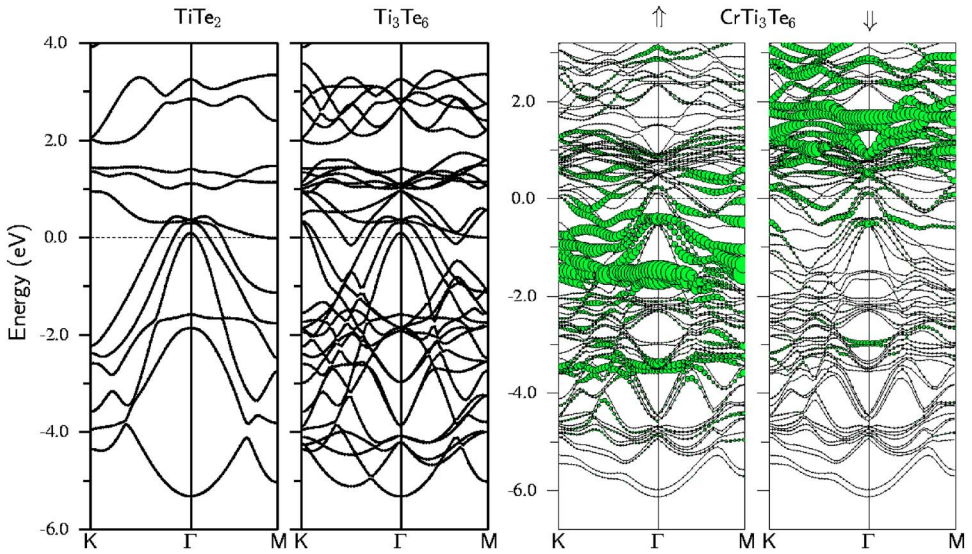

FIG. 3. (Color online) Calculated band dispersions for pure $TiTe_2$ (left-hand panel) and $Cr_{1/3}TiTe_2$ (right-hand two panels). Zero energy is at the Fermi level; note its shifting upwards, relative to the valence band minimum, on doping with Cr. The second panel shows the bands calculated for pure $TiTe_2$ in the tripled cell, identical to that used for the case of the Cr doping. The labeling of the BZ corresponds to the single cell. An artificial broadening of bands in the case of $Cr_{1/3}TiTe_2$ highlights the contributions of the Cr3*d* states with two spin directions over the otherwise common (because of the spin-orbit interaction included) band structure—see text for details.

$=0.257\,63$ for $Cr_{1/3}TiTe_2$, where z is the relative Ti-Te interplane distances. Previous calculations of the band structure of $TiTe_2$ have been reported by de Boer *et al.*[14] and later performed by Eyert.[15] Following these studies, which were limited by the atomic sphere approximation and the neglect of the spin-orbit coupling, a pseudopotential calculation with Gaussian-type orbitals and spin-orbit interaction included has been reported in Ref. 16. We use at present an all-electron method, that however does not lead to any noticeable differences in the energy dispersion as compared to that of Ref. 16.

In order to account for the lattice distortion around intercalate atoms, we allowed a conjugate-gradient search making use of the forces acting on all atoms, thus optimizing all free coordinates in the supercell. The (experimental) lattice constants were assumed to remain unchanged. The net effect of relaxation is a noticeable (by about 1.5%) flattening of the Te octahedron around the intercalated Cr, so that the adjacent Ti-centered octahedra are enlarged correspondingly. The edges of the upper and lower Te triangles neighboring the Cr atom actually grow from 3.873 to 3.872 Å; however, because of the mentioned flattening, the Cr-Te distance decreases from 2.709 Å to 2.693 Å. The distance between the intercalated Cr and the Ti atom, neighboring to the latter in the z direction, gets shortened by about the same relative amount (of about 0.6%), namely from 3.173 to 3.155 Å. This apical Ti atom remains roughly in the middle of its enlarged octahedron.

The calculated band structure for the relaxed supercell is shown in Fig. 3, right-hand panel. It should be noted that the difference from the results for the unrelaxed case are not noticeable on this energy scale. As the calculation included taking spin-orbit coupling into account, the band structure cannot be separated into majority-spin and minority-spin dispersion plots. Two rightmost panels of Fig. 3 show therefore the same band structure, but differently decorated (by colored circles of different size) according to the contribution of the Cr3$d\uparrow$ and Cr3$d\downarrow$ states over different parts of the Brillouin zone. As a crude simplification, one notes a spin-split group of rather flat bands. Those in the majority-spin ($\uparrow$) channel lie by $\sim$1.7 eV below the Fermi level, the minority-spin ($\downarrow$) ones by $\sim$1.9 above E_F. The flatness of these bands manifests the fact that the Cr atoms are far separated in the lattice. Yet, the hybridization of Cr3*d* with the Te5*p*-Ti3*d* valence band mediates the interaction of "highlighted" states, yielding them some dispersion within the energy interval of 1 eV or so. The leftmost panel of Fig. 3 shows the band structure of pure $TiTe_2$, plotted along the *K*-Γ-*M* directions of the nominal BZ, shown in the top right-hand side of Fig. 1. The second panel from the left-hand side shows essentially the same band structure, calculated along the same directions in the **k** space, but for the tripled unit cell, hence the large number of backfolded bands. Comparing the band structures of Ti_3Te_6 and $CrTi_3Te_6$, one can clearly see the effect of Cr intercalation. First there is a shift of the Fermi level by $\sim$0.8 eV with respect to the valence band top, due to extra electrons provided to the system. The Cr3*d* electrons are accommodated in the previously mentioned flat band. The presence of the latter modifies the bands near the valence band top, which are of predominantly Ti3*d* character. The decomposition of different bands by symmetry is further explained by Fig. 4, which contains the local 3*d* densities of states (DOS) at the Cr site and at the Ti closest to it in the z direction. (The local DOS at the other Ti position looks very much the same.) Moreover, the splitting into d_{z^2}, $(d_{x^2-y^2}+d_x)$, and $(d_{xz}+d_{yz})$ components, different by symmetry in the hexagonal crystal field, is shown. The d_{z^2} orbitals at the Cr and Ti sites, pointing to each other through the triangle of chalcogens (see Fig. 1), exhibit similar features in their corresponding DOS within $-1-2$ eV around the Fermi level.

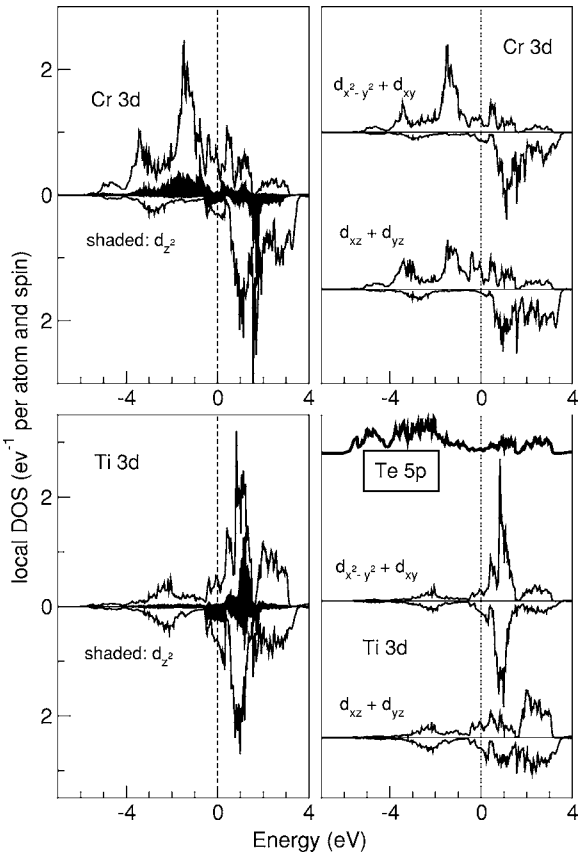

FIG. 4. Calculated 3*d* local density of states for Cr (top panel) and Ti, nearest to the intercalated Cr (bottom panel), each resolved into three contributions split by the crystal field. The Te5*p* DOS is also shown for comparison.

Moreover, they are decidedly more narrow, in the energy domain, than both the $d_{x^2-y^2}+d_{xy}$ and $d_{xz}+d_{yz}$ partial DOS at each respective center, an indication of their higher spatial localization. The interaction with the Te5*p* states is rather weak for Cr and Ti d_{z^2} orbitals. As particularly the Cr3*d* states are expected to be relatively localized, the treatment of correlation effects in this shell within the conventional DFT approach may not be adequate. A more sophisticated analysis beyond the DFT might affect the results in a noticeable way, e.g., enhancing the spin splitting of Cr3*d* states. However, present-day methods of treating such effects in a first-principle calculation, like LDA+U,[17] rely in practice on a clear-cut *a priori* selection of states declared as correlated ones, and on the choice of the average Coulomb interaction parameter, U, for these states. None is obvious for the present system, where Cr3*d* states are by far less localized than in typical correlated oxides. These effects may deserve a special more detailed study in the future.

IV. RESULTS AND DISCUSSION

Figure 2 shows the variation of a, c lattice parameters of powder $TiTe_2$ samples in their dependence on the concentration of inserted Cr.[18] In the region $0.05<x<0.33$, c_0 decreases monotonically. Such behavior was earlier observed in other materials where the intercalation leads to a localization of electronic states.[2] Therefore one can anticipate localization effects in the electronic structure of $Cr_{1/3}TiTe_2$. An increase in c_x for $x>0.33$ was observed in Cr_xTiSe_2 and explained by a broadening of the hybridized band at large impurity concentrations due to an overlap of orbitals at adjacent impurity centers.[19]

The dispersion curves from the ARPES have been constructed using the standard procedure.[20] The wave-vector component parallel to surface is determined by

$$k_{\|}(\text{Å}^{-1}) = 0.512[E_{\text{kin}}(\text{eV})]^{1/2} \sin\Theta,$$

where the kinetic energy of the photoelectron is $E_{\text{kin}}=h\nu-E_b-\phi$, with $h\nu$, E_b, and ϕ denoting the photon energy, the binding energy, and the sample work function, respectively. The $k_{\|}$ of the electron momentum **k** is conserved on exit from the sample into the vacuum, due to two-dimensional translation symmetry of crystal. However the normal component $k_{\perp}$ does not have to be conserved. In order to determine this latter component, one needs to know the energy dispersion $E(k_{\perp})$ of unoccupied states inside the crystal, for which purpose one often abides by the free-electron approximation. The angle-resolved photoelectron emission allows one to find $E(\mathbf{k})$ by tracing the energies of spectral peaks in their dependence on **k**. In doing this one can vary both $k_{\|}$ (by scanning the emission angle) and $k_{\perp}$ (by changing excitation energy). Therefore an experiment performed with varying the $k_{\|}$ only would not suffice to control the total wave vector of an electron, **k**. Special methods have been developed for resolving the energy dispersion in three-dimensional wave vector.[20–23] In the case of quasi-two-dimensional materials, like 1*T*-$TiTe_2$ and Cr_xTiTe_2, it can be assumed that the energy dependence on the normal k component will be negligible.[15] However, this assumption has been revised in some works.[15,16] Rossnagel *et al.*[16] have shown that the $k_{\perp}$ component is not negligibly small. It should be noted that a decrease of the lattice parameter on intercalation makes the crystal more dense and less "quasi-two-dimensional," than it could have been implied for pure $TiTe_2$.

Figure 5 shows the energy distribution curves of 1*T*-$TiTe_2$ for $k_{\|}$ points along the Γ-M (A-L) direction. The experimental peak positions are indicated by tic marks. The normal emission corresponds to Γ ($k_{\|}=0$). All spectra contain a peak just below the Fermi edge, whose intensity rises with increasing $k_{\|}$ so potently that the detector gets saturated, and spectra are arbitrarily cut in Fig. 5. Such dependence of this peak's intensity, and also of its width, on $k_{\|}$ are consistent with earlier reported data.[14–16] The pinned energy position of the peak reveals a dispersionless band, which is not revealed in DFT calculation. Apart from this, the dispersion of other local maxima in angle-resolved spectra of $TiTe_2$ falls astonishingly well onto the calculated DFT band structure, as will be discussed in a minute.

We turn now to the similar spectra for the $Cr_{1/3}TiTe_2$ system, measured along Γ-M and Γ-M', and shown in Fig. 6. The peak intensities at M and M' are different because of different emission depth from Te atoms, which contribute to the spectra detected along these two directions—see a more detailed discussion below. In both panels of Fig. 6, an almost

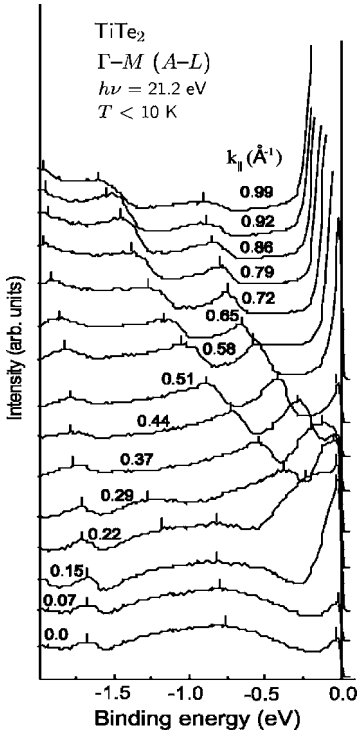

FIG. 5. A sequence of $TiTe_2$ spectra, measured for different values of $k_\parallel$ and hence scanning the Γ-M (or A-L) direction of the BZ. The tic marks indicate peak positions, shown in Fig. 9 (left-hand panel). The spectra are cut in the vicinity of the Fermi level, where their intensity was artificially truncated by the detector's saturation.

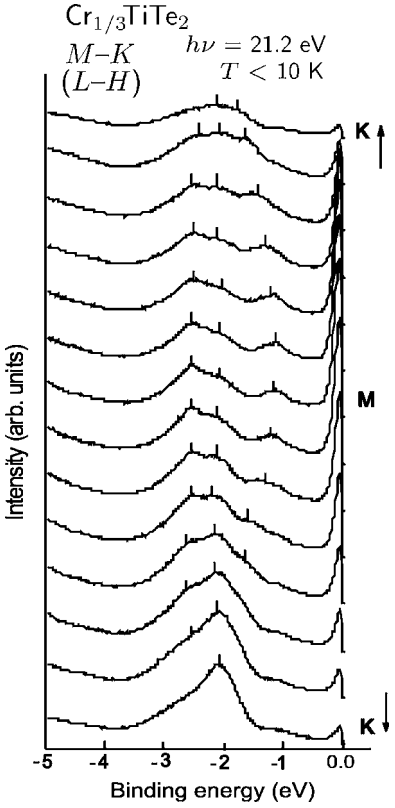

FIG. 7. Similar to Fig. 6, measured along the M-K (or L-H) direction of the BZ for small emission angles.

dispersionless band, not present in pristine $TiTe_2$, is seen at about 1 eV below the Fermi level. However, no such feature is observed in the spectra corresponding to the M-K (L-H) direction, as is obvious from Fig. 7. A dispersionless character of this band implies that the electrons in the corresponding states are localized. If the localization was due to structural defects, e.g., a mere presence of intercalating Cr, the dispersionless band would be isotropic over the Brillouin zone.[24] An observed extremely anisotropic character is a signature of a polaron band.[6] The most prominent difference between the spectra probing the Γ-M and the Γ-M' directions of the BZ is the presence of an intense peak just below

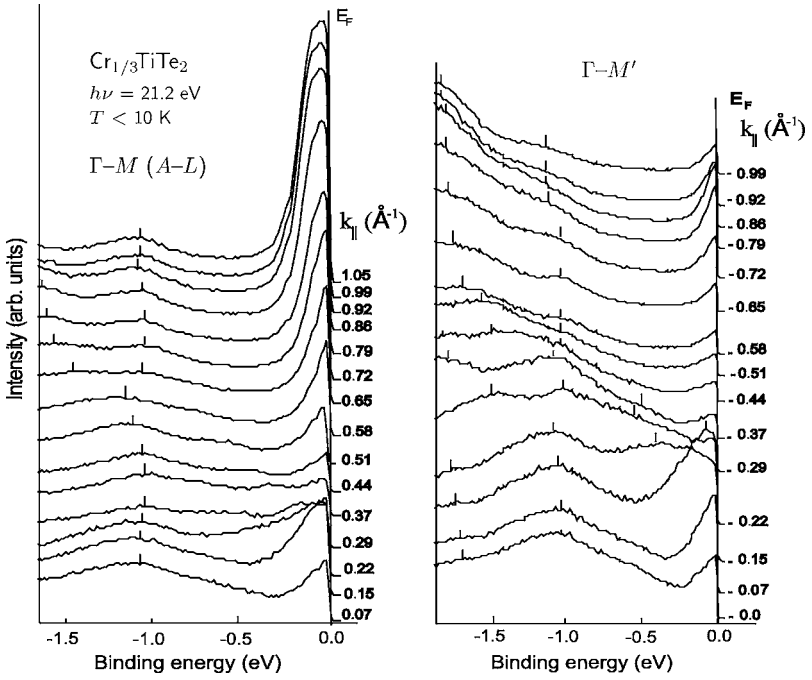

FIG. 6. Angle-resolved energy distribution curves of $Cr_{1/3}TiTe_2$ measured along the Γ-M (A-L) and Γ-M' high-symmetry directions of the BZ, with the He_I radiation at 10 K. $k_\parallel$=0.0 $Å^{-1}$ is the normal emission. High spectral intensity for large $k_\parallel$ values (from $\approx$0.79 $Å^{-1}$) in the left-hand panel was artificially truncated by the detector's saturation. The energy resolution is 5 meV. The ticks in the curves indicate local maxima, the positions of which are represented by circles in Fig. 9 (right-hand panel).

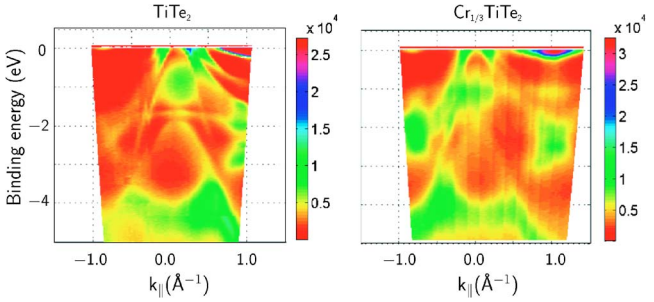

FIG. 8. (Color online) Summary energy distribution of the photoemission intensity from the spectra of Figs. 5 and 6, $I(k_{\|},E_b)$, of pristine and Cr-intercalated $TiTe_2$. Photoemission intensity is represented in a linear color code as indicated by the color bar. In both panels, $k_{\|}$ probes the M'-Γ-M direction of the BZ. The intensity maxima are centered at the M points, which originate from the Ti3d band. The observed difference of intensity between the M and M' points reflects the threefold symmetry of the crystal structure (see text for details).

the Fermi level, which can be assigned to the Ti $3d_{z^2}$-derived conduction band. The actual strong intensity of these peaks actually saturates the detector sensitivity in the spectra shown in Fig. 6, left-hand panel.

Figure 8 summarizes the individual spectra of pristine and Cr-intercalated $TiTe_2$, like those shown in Figs. 5 and 6, but going deeper in binding energies, as a "relief" of intensity over the $(E_b,k_{\|})$ plane. E_b is the binding energy and $k_{\|}$ the wave-vector component parallel to the planar base of the BZ. This presentation facilitates the comparison with calculated band dispersions in Fig. 3. For clarity, the positions of pronounced peaks are separately shown in Fig. 9, and the resulting bands labeled there a to e. The $TiTe_2$ spectrum reveals a band which ascends towards the zone center in a close vicinity of the latter, in the range of binding energies 0.6–1.3 eV. In fact the local maxima in the corresponding energy interval of the spectra are somehow difficult to trace as well pronounced peaks. In the left-hand panel of Fig. 9, this region is marked by a hatched area. This structure has also been reported earlier in Ref. 15, and explained there as being due to the scattering of photoelectrons on phonons. No such feature is seen in calculated band structures (Fig. 3). In both pristine

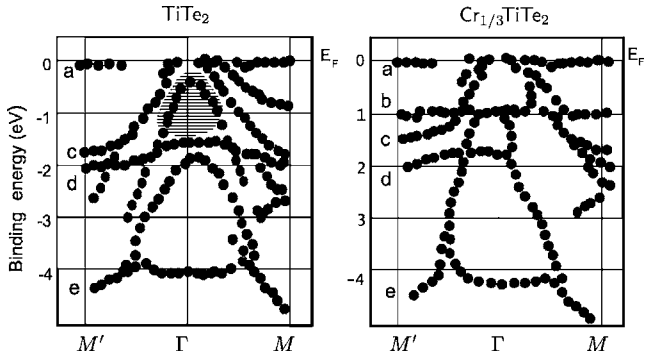

FIG. 9. Dispersions of experimental peak positions from the spectra of Figs. 5 and 6, measured along M'-Γ and Γ-M (A-L) for $TiTe_2$ and $Cr_{1/3}TiTe_2$. The hatched area marks a structure formed by weakly pronounced spectral peaks (see text for details).

and doped compounds the spectra contain a pronounced band a in the vicinity of the Fermi level. Its intensity approaches maximum near the M point and seems to be flat, on approaching M from Γ. This can be understood as the saturation of the photoemission current and indicates a much larger number of electron states in this band as compared to the case of Cr_xTiTe_2. In general, this band exhibits a strong dispersion of intensity with the direction of **k**. It is worth reminding here that the $1T$-$TiTe_2$ structure belongs to a trigonal crystallographic system with third-order inversion axis (space group $P\bar{3}m1$). As was already mentioned above, this trigonality leads to breaking the symmetry of intensity corresponding to M' and M. Geometrical conditions of detecting the spectra are identical for these two points; however, the incidence depths of electrons differ. The Γ-M direction is dominated by electrons ejected from the "upper" parts of the $TiTe_2$ octahedra (i.e., those nearest to the surface of sample) while in the Γ-M' direction the emission comes from the lower parts of the octahedra. The corresponding incidence depths differ by about the $c/2$ parameter of the crystal lattice, with $c=6.491$ Å for $TiTe_2$ and 6.35 Å for $Cr_{1/3}TiTe_2$. The reason for a sharp drop of intensity, as has been shown in Ref. 25, is an efficient scattering of electrons with energies just below E_F, emitted from the lower chalcogen layer, on the upper layer of atoms. The measurements of spatial distribution of the photoemission intensity in Ref. 25 indicated trigonal symmetry of $1T$ and hexagonal for $2H$ polytypes, respectively.

The fact that the M/M' intensities relation remains the same on going from $TiTe_2$ to $Cr_{1/3}TiTe_2$ indicates the survival of the third-order rotational symmetry in the course of intercalation. This justifies the choice of a supercell for the electronic structure calculation of $Cr_{1/3}TiTe_2$, as discussed above.

In both materials a hole pocket of the Fermi surface exists in the vicinity of Γ formed by a band that bends upwards by 0.3 eV to above the Fermi level. The electronic structure calculations help to identify this band as being formed by three hybridized Tid_{z^2}-Te5p bands (Fig. 3). Its intensity is higher in pristine $TiTe_2$ than in the intercalated compound, probably because there are two bands c and c' (along the $M\rightarrow\Gamma$ line) in $TiTe_2$, which become degenerate in Γ, whereas in $Cr_{1/3}TiTe_2$ there is only one band symmetrically crossing the Fermi level (Fig. 8). It is noteworthy that the intercalation does not increase the binding energy of electron-type bands, nor that of hole-type bands. That is why the intercalation with Cr does not change the half-metallic nature of $TiTe_2$, similarly as the intercalation with Eu does not change it in $TiSe_2$.[26]

The structures in the bonding energies region beyond 2 eV are mostly formed by the Te5p states, as was already known from earlier calculations.[15,16] Whereas the composition of bands remains the same in pristine and intercalated compounds, the contrast is better in $TiTe_2$. Their shape, incidentally symmetric around Γ in the undoped compound, gets substantially distorted on intercalation with Cr (the band d). In our opinion this can be related to nonstoichiometry, and consequently the presence of defects, in the intercalated compound. All observed $E(\mathbf{k})$ dependencies imply contribu-

tions from $E(k_\perp)$; this is the most obvious for the bands near M and M' with binding energies of about 2 eV that closely resemble the same in $TiTe_2$ (Fig. 8). This is detected for both materials. A similar band appears at Γ around the binding energy of 1 eV, somehow washed out in an intercalate material.

The whole region of detected angles is spanned by a dispersionless band *b* at the binding energy if about 1 eV (Figs. 8 and 9), similar to that observed in Ref. 3 for $Ni_{1/3}TiS_2$, $Co_{1/3}TiS_2$ (Ref. 2) and in Refs. 14, 27, and 28 for titanium dichalcogenides contaminated by overstoichiometric Ti. Apparently this band appears due to hybridization of Ti3*d* and Cr3*d* states.

The presence of a hybrid state band is in accordance with band calculation results (Fig. 3). However, the observed band differs from the calculated one. First, the width of the calculated band is about 0.5 eV, while no such dispersion was observed in the spectra. Second, the experimental binding energy of this band is smaller than the calculated one by about 0.5 eV. We suggest that these discrepancies may be explained by assuming a substantial polaron character of the band in question. When referring to a polaron in this context, we imply an electron localized on a Ti-Cr-Ti complex and polarizing the lattice. It can be seen from Fig. 2 that the insertion of Cr induces the lattice compression along the *z* axis. (In the case when electrons remain unbound and do not polarize the lattice, that is, e.g., the case of doping with alkali metals, the lattice deformation has an opposite sense.) Moreover, as Cr atoms tend to order or at least to take evenly spaced interstitial positions, a sublattice is formed along which the localized electrons may travel. Under the assumption about the polaron character of the band, an absence of dispersion in the latter is due to the lattice screening of Ti-Cr-Ti triads, so that they become effectively noninteracting. A smaller measured binding energy of the band, as compared to the calculation result, can also be caused by a screening of the Ti-Cr-Ti "impurities," which leads to a decrease of their effective ionization potential. An observed lattice compression during Cr insertion does qualitatively confirm a suggested polaron origin of this band. The relaxation of local structure in the course of *ab initio* calculations indicates that the Ti atom, close to the intercalating Cr atom, displaces towards the latter. Qualitatively this is consistent with the assumption about the polaronic nature of hybridized Ti3*d*-Cr3*d* states. However, the magnitude of calculated displacement is too small to have a noticeable effect on the band structure. It does not result in unambiguous narrowing of the band under discussion and in increasing its binding energy. This trend might become more pronounced if correlation effects are treated beyond the conventional DFT scheme, because such treatment is likely to result in an enhanced localization of involved states.

In conclusion, the change in the photocurrent intensity in M due to intercalation with Cr agrees well with the assumption about localized character of hybridized Cr3*d*-Ti3*d* states. Indeed, it was shown in Ref. 29 that the formation of hybrid states leads to switching the titanium *d* states from the Ti3d_{z^2} into the hybridized Cr3d_{z^2}-Ti3d_{z^2} band. Consequently the formation of the latter must be accompanied by a reduction of the state density in the Ti3*d* and, probably, in the Te5*p* bands. We note a relatively low intensity of this band, related, to our opinion, to spin polarization of Cr3*d* electrons. A comparison with band structure calculations fully supports this assumption.

V. CONCLUSIONS

A comparison of ARPES spectra from the intercalated $Cr_{1/3}TiTe_2$ and the parent $TiTe_2$ compounds shows that an insertion of Cr leads to formation of a narrow almost nondispersion band, lying at about 1 eV below the Fermi level. This result is in a good accordance with the data known for other intercalation materials, where an appearance of such bands was demonstrated every time there was an effect of lattice compression in the direction normal to the basis plane upon intercalation. A comparison with band calculations allows one to identify this band as a band of hybrid Cr3*d*-Ti3*d* states. However, the experimentally determined width of this band is almost two times smaller than for the theoretically predicted one. We suggest that this discrepancy is connected with a polaron origin of states of the mentioned band.

ACKNOWLEDGMENTS

This work was supported by the Russian Federation for Basic Research, Grant No. 04-03-96083-p2004ural. The funding by the Research Council of the President of Russian Federation (Grant No. NSH-1026.2003.2) is appreciated. We also gratefully acknowledge financial support by the Deutsche Forschungsgemeinschaft.

*Also at: Ural State University, 620083 Yekaterinburg, Russia.

†Also at: Institut für Festkörperforschung, Forschungszentrum Jülich, D-52425 Jülich, Germany.

‡Present address: Universität Würzburg, Experimentelle Physik II, Am Hubland, D-97074 Würzburg, Germany.

[1] A. N. Titov, A. V. Dolgoshein, I. K. Bdikin, and S. G. Titova, Phys. Solid State **42**, 1610 (2000).

[2] T. Matsushita *et al.*, J. Electron Spectrosc. Relat. Phenom. **78**, 477 (1996).

[3] T. Matsushita, S. Suga, A. Kimura, H. Negishi, and M. Inoue, Phys. Rev. B **60**, 1678 (1999).

[4] M. Inoue, H. P. Hughes, and A. D. Yoffe, Adv. Phys. **38**, 565 (1989).

[5] K. Gofron, J. C. Campuzano, A. A. Abrikosov, M. Lindroos, A. Bansil, H. Ding, D. Koelling, and B. Dabrowski, Phys. Rev. Lett. **73**, 3302 (1994).

[6] A. S. Alexandrov and N. F. Mott, *Polarons and Bipolarons* (World Scientific, Singapore, 1996).

[7] A. N. Titov and A. V. Dolgoshein, Phys. Solid State **42**, 434 (2000).
[8] A. N. Titov, A. V. Kuranov, V. G. Pleschev, Y. M. Yarmoshenko, M. V. Yablonskikh, A. V. Postnikov, S. Plogmann, M. Neumann, A. V. Ezhov, and E. Z. Kurmaev, Phys. Rev. B **63**, 035106 (2001).
[9] F. Reinert, G. Nicolay, S. Schmidt, D. Ehm, and S. Hüfner, Phys. Rev. B **63**, 115415 (2001).
[10] P. Blaha, K. Schwarz, G. K. H. Madsen, D. Kvasnicka, and J. Luitz, WIEN2K, Vienna University of Technology, 2001, improved and updated Unix version of the original copyrighted WIEN code, which was presented by P. Blaha, K. Schwarz, P. Sorantin, and S. B. Trickey, Comput. Phys. Commun. **59**, 339 (1990), URL http://www.wien2k.at
[11] J. P. Perdew, K. Burke, and M. Ernzerhof, Phys. Rev. Lett. **77**, 3865 (1996).
[12] A. V. Postnikov, M. Neumann, S. Plogmann, Y. M. Yarmoshenko, A. N. Titov, and A. V. Kuranov, Comput. Mater. Sci. **17**, 450 (2000).
[13] N. Suzuki, T. Yamasaki, and K. Motizuki, J. Phys. Soc. Jpn. **58**, 3280 (1989).
[14] D. K. G. de Boer, C. F. van Bruggen, G. W. Bus, R. Coehoorn, C. Haas, G. A. Sawatzky, H. W. Myron, D. Norman, and H. Padmore, Phys. Rev. B **29**, 6797 (1984).
[15] R. Claessen *et al.*, Phys. Rev. B **54**, 2453 (1996).
[16] K. Rossnagel, L. Kipp, M. Skibowski, C. Solterbeck, T. Strasser, W. Schattke, D. Voß, P. Krüger, A. Mazur, and J. Pollmann, Phys. Rev. B **63**, 125104 (1999).
[17] V. I. Anisimov, F. Aryasetiawan, and A. I. Lichtenstein, J. Phys.: Condens. Matter **9**, 767 (1997).
[18] The lattice remains hexagonal up to $x=0.5$, at which concentration the intercalated chromium forms a monoclinically ordered superstructure, as mentioned in Sec. II. The lattice parameters of Fig. 2 are shown in the hexagonal setting throughout, e.g., for $x=0.5$ as derived from the corresponding monoclinic lattice parameters.
[19] A. N. Titov, Y. M. Yarmoshenko, M. Neumann, V. G. Pleschchev, and S. G. Titova, Fiz. Tverd. Tela (S.-Peterburg) **46**, 1628 (2004).
[20] S. Hüfner, *Photoelectron Spectroscopy: Principles and Applications*, Springer Series in Solid-State Sciences, Vol. 82 (Springer-Verlag, Berlin, 1995).
[21] V. N. Strocov *et al.*, Phys. Rev. Lett. **81**, 4943 (1998).
[22] V. N. Strocov *et al.*, Phys. Rev. B **63**, 205108 (2001).
[23] M. Bovet, V. N. Strocov, F. Clerc, C. Koitzsch, D. Naumović, and P. Aebi, Phys. Rev. Lett. **93**, 107601 (2004).
[24] H. E. Brauer, H. I. Starnberg, L. J. Holleboom, H. P. Hughes, and V. N. Strocov, J. Phys.: Condens. Matter **11**, 8957 (1999).
[25] N. V. Smith and M. M. Traum, Phys. Rev. B **11**, 2087 (1975).
[26] S. Danzenbacher, S. L. Molodtsov, K. Koepernik, Y. Tomm, and C. Laubschat, Mol. Cryst. Liq. Cryst. Sci. Technol., Sect. A **341**, 849 (2000).
[27] J. J. Barry, H. P. Hughes, P. C. Klipstein, and R. H. Friend, J. Phys. C **16**, 393 (1983).
[28] C. H. Chen, W. Fabian, F. C. Brown, K. C. Woo, B. Davies, B. DeLong, and A. H. Thompson, Phys. Rev. B **21**, 615 (1980).
[29] A. N. Titov and A. V. Dolgoshein, Phys. Solid State **40**, 1081 (1998).